




The effect of $(\text{Bi}_{0.5}\text{Li}_{0.5})_{0.9}\text{Sr}_{0.1}\text{ZrO}_3$ substitution on the construction of polymorphic phase boundary and high curie temperature of $\text{K}_{0.45}\text{Na}_{0.55}\text{NbO}_3$ piezoelectric ceramics

Ruihua Zheng¹, Qiyi Yin^{1*} , Hengwen Cheng¹, Xianzhao Zhang¹, Kunhong Hu¹, Fei Lin¹, Yulin Zhang¹, Shicheng Wang¹, Zhen Zhang¹, and Quanzheng Zhang¹

¹ School of Energy Materials and Chemical Engineering, Hefei University, 230601 Hefei, People's Republic of China

Received: 8 February 2023

Accepted: 21 March 2023

Published online:
13 April 2023

© The Author(s), under exclusive licence to Springer Science+Business Media, LLC, part of Springer Nature 2023

ABSTRACT

In this experiment, new high-temperature piezoelectric ceramics $(1-x)\text{K}_{0.45}\text{Na}_{0.55}\text{NbO}_3-x(\text{Bi}_{0.5}\text{Li}_{0.5})_{0.9}\text{Sr}_{0.1}\text{ZrO}_3$ were prepared by the conventional solid-state sintering method, and the effect of the doping amount of $(\text{Bi}_{0.5}\text{Li}_{0.5})_{0.9}\text{Sr}_{0.1}\text{ZrO}_3$ on the microstructure and electrical properties of this system ceramics were systematically investigated. XRD, SEM, EDS, and other modern test technology analysis results show that all the doped ions have entered the KNN lattice in the studied range, forming a dense solid solution with a pure perovskite structure, and forming orthorhombic–tetragonal polymorphic phase boundaries at $0.02 \leq x \leq 0.035$, the ceramics exhibit rhombohedral–tetragonal polymorphic phase coexistence in the range of $0.04 \leq x \leq 0.05$. The electrical properties tests show that the ceramics of this system exhibit excellent electrical properties in the multiphase coexistence region at $x = 0.04$, which are: $d_{33} = 307 \text{ pC/N}$, $k_p = 46\%$, $\epsilon_r = 1363$, $\tan\delta = 2.79\%$, $P_r = 16.7 \text{ } \mu\text{C/cm}^2$, $E_c = 12.65 \text{ kV/cm}$, and $T_c = 368 \text{ }^\circ\text{C}$. These excellent electrical properties and the high Curie temperature predict that the ceramics of this system have great prospects for future applications in the field of lead-free piezoelectric ceramics.

1 Introduction

In recent years, there has been great progress in the modification research for potassium sodium niobate (KNN) based ceramics, especially through the substitution of A- and B-site ions to optimize the

components and adjust the phase boundaries to appear to have multiple phases coexisting close to room temperature, such as R–O and O–T, which can significantly enhance the piezoelectric properties of KNN-based lead-free ceramics but still cannot be compared with commercial PZT ceramics in the

Address correspondence to E-mail: yinqiyi@hfu.edu.cn

overall performance [1–8]. In order to achieve superior piezoelectric properties in 2016, Xu et al. created the ceramics system KNNS-BZ-BKH and successfully designed a new R–T ceramic phase boundary, proving that the existence of R–T phase boundaries is a proven method to improve the performance of KNN-based piezoelectric ceramics [9]. However, this method typically results in a large reduction in T_C and an improvement in the piezoelectric characteristics of KNN-based ceramics [10–12]. It is therefore difficult to enhance the piezoelectric qualities without decreasing the T_C , necessitating the construction of an entirely new system to solve both problems simultaneously [13–15].

In recent years, many studies have confirmed that the construction of new phase boundaries in KNN-based piezoelectric ceramics is conducive to the enhancement of piezoelectric performance, but it will also lead to a significant decrease in the Curie temperature. In this experiment, the introduction of the second component $(\text{Bi}_{0.5}\text{Li}_{0.5})_{0.9}\text{Sr}_{0.1}\text{ZrO}_3$ in KNN-based ceramics mainly has the following reasons, first of all, we choose to doping Li ions can effectively enhance the sintering activity of KNN-based ceramics, so that the density of ceramics is improved, and it is conducive to improving the Curie temperature of ceramics [16, 17]. Secondly, doping $(\text{Bi}_{0.5}\text{Na}_{0.5})\text{ZrO}_3$ in KNN-based ceramics can increase the rhombohedral–orthorhombic phase transition temperature (T_{R-O}), and also reduce the orthorhombic–tetragonal phase transition temperature (T_{O-T}), thereby effectively construct a new R–T phase boundary [15, 18]. Finally, the use of Sr^{2+} doping with a similar radius to the A ion can effectively control the T_{R-T} phase transition to stabilize to room temperature, while well reducing the O–T phase transition temperature, at present, many related studies report that this polymorphic phase boundary adjustment to near room temperature can make ceramics have more unstable polarization state, so ceramics in the polarized state of ceramic domain flipping is easier, thereby improving the piezoelectric properties of ceramics [19, 20]. In this experiment, the group designed new $(1-x)\text{K}_{0.45}\text{Na}_{0.55}\text{NbO}_3-x(\text{Bi}_{0.5}\text{Li}_{0.5})_{0.9}\text{Sr}_{0.1}\text{ZrO}_3$ ceramics system and systematically investigated the correlation mechanism between the microstructure and electrical properties of the ceramics. This was done with the goal of constructing a new R–T phase boundary without lowering the Curie temperature.

2 Experimental procedure

In this experiment, new lead-free piezoelectric ceramics $(1-x)\text{K}_{0.45}\text{Na}_{0.55}\text{NbO}_3-x(\text{Bi}_{0.5}\text{Li}_{0.5})_{0.9}\text{Sr}_{0.1}\text{ZrO}_3$ [abbreviated as KNN- x BLSZ] ($x = 0, 0.02, 0.03, 0.035, 0.04, 0.05, 0.06$) were prepared by the conventional solid-phase reaction route. The raw materials used in the experiments were as follows: K_2CO_3 (99%), Na_2CO_3 (99.8%), Nb_2O_5 (99.5%), Li_2CO_3 (98%), SrCO_3 (99%), Bi_2O_3 (99.99%), and ZrO_2 (99%). The mass of the necessary raw materials were calculated using the stoichiometric ratio and weighed using a balance. These weighed powders were then ball-milled in an ethanol medium for 12 h, placed in a high-temperature furnace for 6 h at 850 °C for pre-combustion, added 8 to 10 wt% of PVB for granulation and pressing, and then heated for 4 h at 600 °C to release gum and all samples were calcined at 1090–1150 °C for 3 h, after all samples were poled in silicone oil at 120 °C under a DC electric field of 3–4 kV/mm for 30 min. Finally, the performance was evaluated following a 24 h period of rest [21].

The Archimedes method was used to determine the bulk density of ceramics, the phase structure of ceramics was examined by X-ray diffraction (XRD) using $\text{Cu } K\alpha$ radiation (Rigaku, Tokyo, Japan), the surface micromorphology of ceramics was characterized by scanning electron microscopy (SEM) (S-4800, Hitachi, Japan), in order to test the dielectric constant and dielectric loss of ceramics in the temperature range of -150 to 100 °C and room temperature to 500 °C, and the surface microscopic morphology was assessed using an LCR meter (HP4980A, Agilent, USA). A piezo- d_{33} meter (ZJ-3 A, China Institute of Acoustics) and an impedance analyzer were used to measure the piezoelectric constant d_{33} and the planar electromechanical coupling factor k_p (HP4294A, Agilent, USA). The hysteresis lines were measured at room temperature using a ferroelectric measurement system (Trek 609B, Radiant Technologies, Inc. Albuquerque) [21].

3 Results and discussion

All ceramics samples are solid solutions with a pure perovskite structure, as shown by the XRD patterns measured at room temperature for KNN- x BLSZ ceramics ($2\theta = 20^\circ$ – 60°) in Fig. 1a. This along with the results of the EDS test in Fig. 6, suggests that BLSZ

has been fully incorporated into the KNN lattice. The main reason for this result is that the ions at the A and B sites have similar ionic radii, Bi^{3+} ($R_{\text{Bi}^{3+}} = 0.145 \text{ nm}$), Li^+ ($R_{\text{Li}^+} = 0.125 \text{ nm}$), Sr^{2+} ($R_{\text{Sr}^{2+}} = 0.144 \text{ nm}$) with A-site K^+ ($R_{\text{K}^+} = 0.164 \text{ nm}$), Na^+ ($R_{\text{Na}^+} = 0.139 \text{ nm}$), Zr^{4+} ($R_{\text{Zr}^{4+}} = 0.072 \text{ nm}$) with B-site Nb^{5+} ($R_{\text{Nb}^{5+}} = 0.064 \text{ nm}$), they all conforms to the law of fusion of doped ions of solid solution [22, 23]. The XRD diffraction peaks at diffraction angles 43.5° – 47.5° are magnified in Fig. 1b, and it is clear that as x is gradually increased, the peak pattern of the system ceramic at these angles considerably changes, the peak pattern of the system ceramic at diffraction angles 43.5° – 47.5° changes significantly. Two distinct subpeaks (002) and (020) can be seen at 45° when $x = 0$. The (002) peak has a significantly higher intensity than the (020) peak, and its $I(002)/I(020)$ ratio is approximately 2:1, which is typical of the presence of orthorhombic (O) phase in KNN ceramics [24, 25]. When $x = 0.02$ – 0.035 , the intensity of the (002) and (020) diffraction peaks is approximately 1:1, when the ceramics are O–T coexistence, this conclusion has been reported reasoning [26]. In order to better determine, the XRD data was refined using MAUD program and found that when $x = 0.02$, the proportion of orthorhombic phase is 73.2% and the proportion of tetragonal phase is 26.8%, When $x = 0.04$ – 0.05 , the intensity ratio of (002)/(020) diffraction peaks is 1:2, which can be judged as the coexistence of R–T phase, and the proportion of rhombohedral phase is 26.4% and tetragonal phase is 73.6% when combined with the software refinement $x = 0.04$ [27–29]. When $x = 0.06$

of the ceramics, the R–T phase is suppressed due to the excessive refinement of the grains [30].

To further confirm the effect of $(\text{Bi}_{0.5}\text{Li}_{0.5})_{0.9}\text{Sr}_{0.1}\text{ZrO}_3$ content on the phase transition of the ceramic samples, the curves of the dielectric constant with the temperature at low temperatures (-150 – 100°C) were tested in this experiment at a frequency of 10 kHz. This dielectric temperature spectrum shows that the curves for pure KNN ceramics are in general agreement with those reported in previous articles [4, 31]. As shown in Fig. 2a–g, as $x = 0$ increases to 0.035, there are two distinct dielectric constant anomalies in the range of -150 to 100°C for the ceramic samples, $T_{\text{R-O}}$ at low temperature and $T_{\text{O-T}}$ at high temperature. $T_{\text{R-O}}$ gradually increases while $T_{\text{O-T}}$ moves closer to room temperature [32, 33]. When $x = 0$ – 0.035 , the orthorhombic–tetragonal phase transition temperatures ($T_{\text{O-T}}$) are 202°C , 115°C , 57°C , and 30°C , and the rhombohedral–orthorhombic phase transition temperatures ($T_{\text{R-O}}$) are -112°C , -78°C , -31°C , and -6°C , respectively. When $0.04 \leq x \leq 0.05$ samples, $T_{\text{R-O}}$ and $T_{\text{O-T}}$ move further to lower temperatures, and the two dielectric anomalies peaks are essentially fused into one, at which time the ceramic forms a new phase boundary of R–T at room temperature. At $x = 0.06$, the dielectric peak exhibits suppressed R–T phase structure due to the suppression of the phase boundary caused by the excessive refinement of the ceramic grains [30].

In order to investigate the crystal structure of the ceramics, the Rietveld refinement of the XRD patterns at room temperature for the ceramics with $x = 0.02$, 0.035 , and 0.04 is shown in Fig. 3. By performing $R3m$ (rhombohedral), $Amm2$ (orthorhombic), and $P4mm$ (tetragonal) symmetry models on the coexisting phases analyzed by Rietveld analysis, we can find that the variation analysis of the XRD peak patterns is consistent with the crystal structure parameters, which are shown in Table 1. The results show that there is a good agreement between the intensity distributions of the simulated and experimental results through the Sig and Rw values. In addition, by observing Table 1, it can be found that the O-phase ratios increase with the increase of x , while the corresponding T phase ratio is decreasing.

Figure 4a elucidates the ϵ_r – T curves of $(1-x)\text{K}_{0.45}\text{Na}_{0.55}\text{NbO}_3-x(\text{Bi}_{0.5}\text{Li}_{0.5})_{0.9}\text{Sr}_{0.1}\text{ZrO}_3$ ceramics with dielectric constants measured at 10 kHz in the range of 30 – 450°C . Through the dielectric curves, it can be

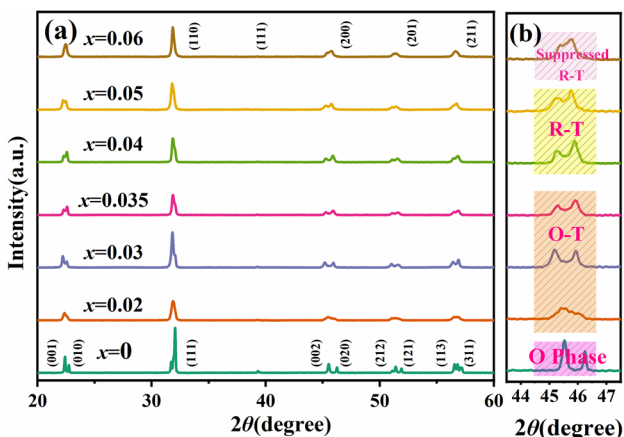


Fig. 1 XRD patterns of the ceramics with **a** $2\theta = 20^\circ$ – 60° , and **b** $2\theta = 43.5^\circ$ – 47.5°

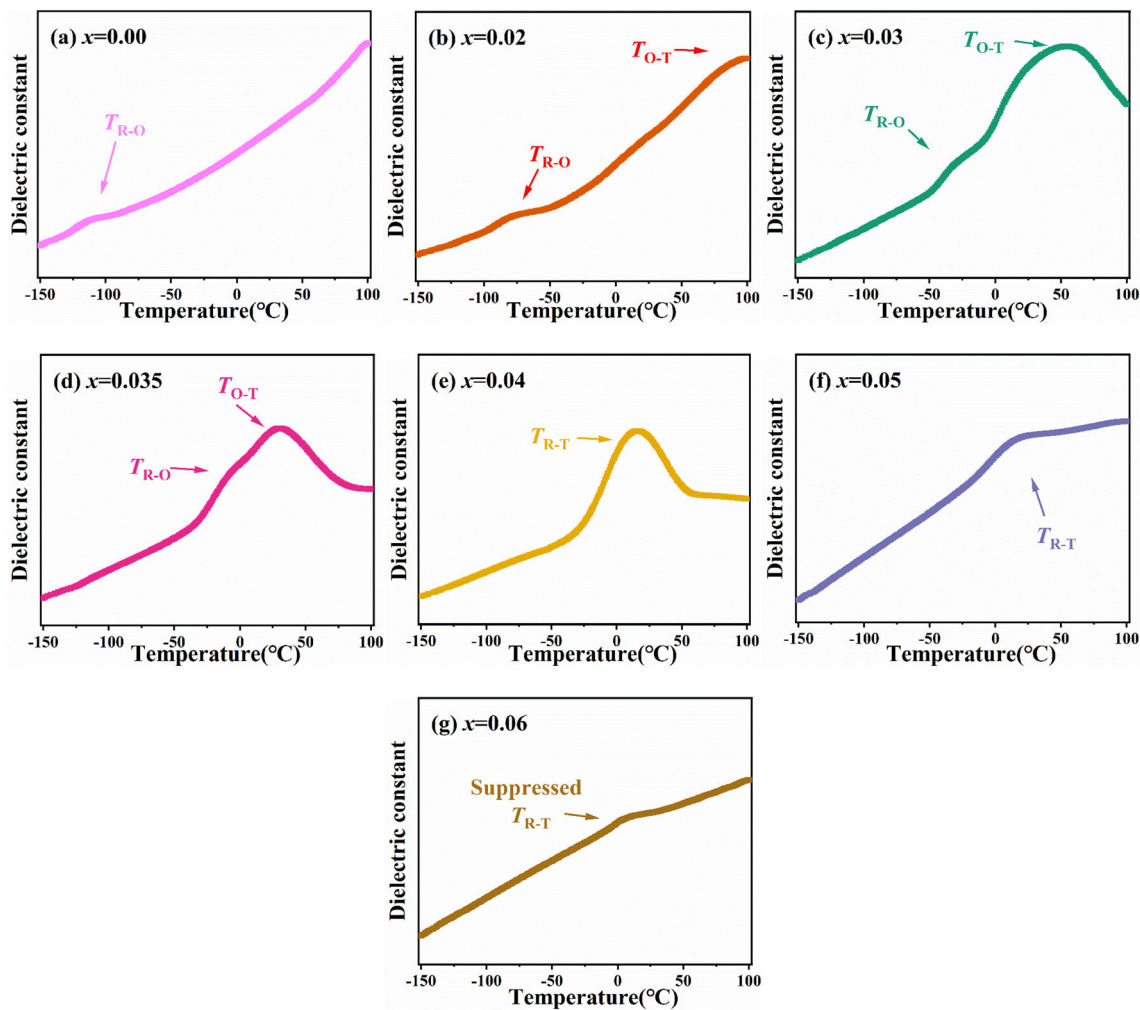


Fig. 2 Dielectric-temperature curves of the ceramics in the temperature range (-150 – 100 °C) with **a** $x = 0.00$, **b** $x = 0.02$, **c** $x = 0.03$, **d** $x = 0.035$, **e** $x = 0.04$, **f** $x = 0.05$, and **g** $x = 0.06$

observed that there is a dielectric peak, whose peak corresponds to the Curie temperature (T_C), and when x is small, the Curie peak is high and narrow, and as x increases, the peak pattern gradually becomes wider, showing the characteristics of diffuse phase transition, which is mainly due to the excessive doping of BLSZ leading to the inhomogeneity of the microscopic region composition, and this inhomogeneity seriously affects the diffusion of the phase transition [34]. From the doping of BLSZ as observed in Fig. 4b, the Curie temperature of the ceramics is reduced, but always remains relatively high, showing excellent Curie temperature $T_C = 368$ °C and electrical properties when $x = 0.04$, implying easier application in high-temperature environments. Figure 4c shows the phase structure of KNN- x BLSZ ceramics, from which it can be seen that the T_C and

T_{O-T} of the ceramics. Decreases with increasing x , while T_{R-O} increases with increasing x . As x increases, the peak slowly approaches the room temperature region and evolves into a new phase boundary from the rhombohedral to the tetragonal ($R-T$) phase near the room temperature when $x = 0.04$ – 0.05 .

Figure 5a–f shows the SEM surface morphology of the KNN- x BLSZ ceramics samples. It can be observed that all ceramics samples have a dense microstructure and no excess impurity phases are produced. When $0 \leq x < 0.04$, it is observed that there are many pores between the grains, the ceramic grain size has a considerable inhomogeneous distribution, and the density of the ceramic is poor. At $x = 0.04$, the ceramic grains have good homogeneity, the pores between the grains are kept at a minimum, the

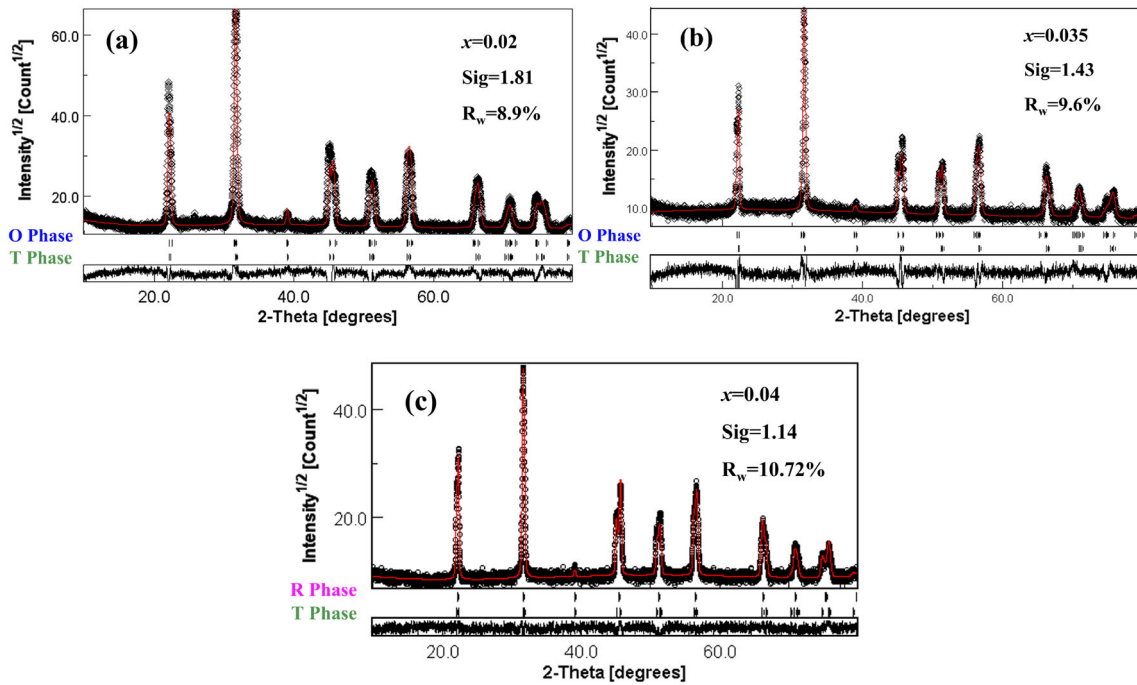
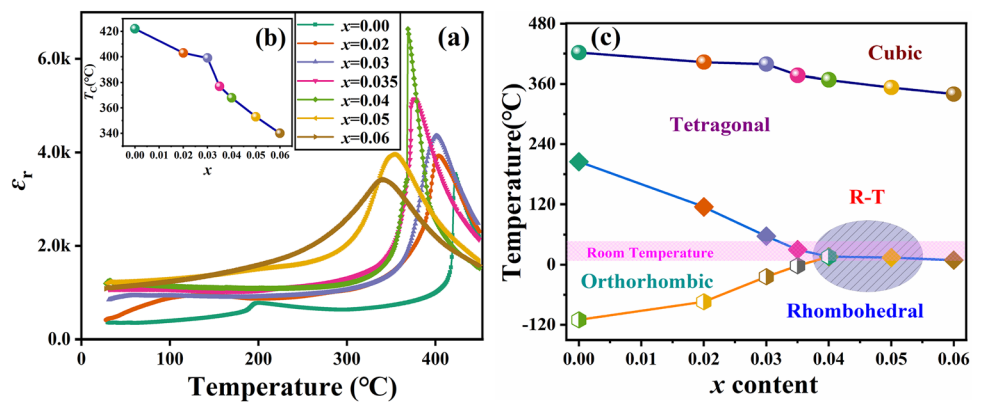


Fig. 3 Rietveld refinement on XRD patterns for a $x = 0.02$, b $x = 0.035$, and c $x = 0.04$

Table 1 Crystal structure parameters of KNN- x BLSZ ceramics

Parameters	$x = 0.02$		$x = 0.035$		$x = 0.04$	
Proportion	73.2%	26.8%	34.6%	65.4%	26.4%	73.6%
Space group	<i>Amm2</i>	<i>P4mm</i>	<i>Amm2</i>	<i>P4mm</i>	<i>R3m</i>	<i>P4mm</i>
a (Å)	3.9450	3.9724	3.9620	3.9864	3.9530	3.9725
b (Å)	5.6644	3.9724	5.6588	3.9864	3.9530	3.9725
c (Å)	5.6802	4.0112	5.7134	3.9639	3.9530	4.2242
α (Å)	90.000	90.000	90.000	90.000	89.650	90.000

Fig. 4 a Temperature dependence dielectric constant of the KNN- x BLSZceramics, b ceramics Curie temperature curve, c the phase diagram of the ceramics



ceramic has good densification, and the domain wall density becomes more homogeneous at this time, which is conducive to the flipping of the electric domains during the polarization process, which improves the electrical properties. When

$0.04 < x \leq 0.06$, combined with the density analysis in Fig. 9, there is a tendency for the pores between the grains to increase, the density of the ceramic decreases, and the ceramic grains start to refine, which is because Bi^{3+} and Zr^{4+} ions tend to

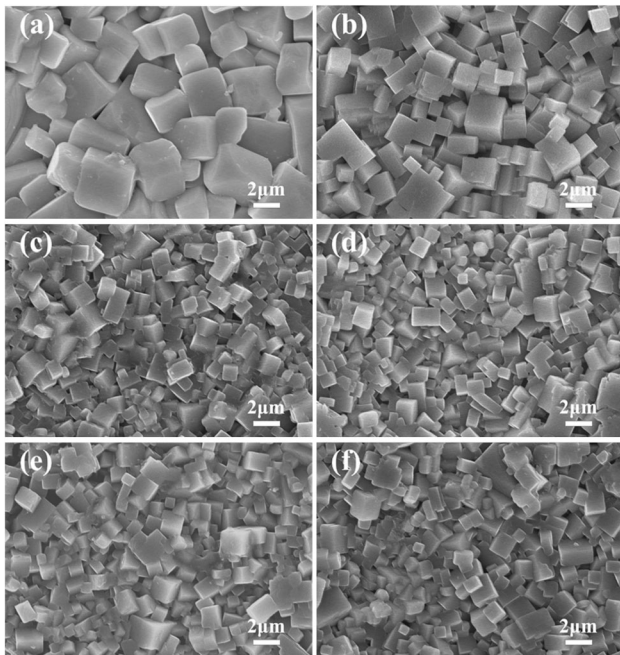


Fig. 5 SEM micrographs of the ceramics: **a** $x = 0.00$, **b** $x = 0.02$, **c** $x = 0.03$, **d** $x = 0.04$, **e** $x = 0.05$, and **f** $x = 0.06$

accumulate at the grain boundaries, making it more difficult for the grain boundaries to move, which hinders the growth of the ceramic grains, resulting in a rise in non-uniform nucleation points, which hinder grain growth during sintering and lead to excessive refinement, which diminishes sintering activity, intensifies pores in the ceramic, and makes domain flipping more complicated during polarization [19, 35, 36]. The sintering activity is reduced, the porosity within the ceramics is increased, and the electric domain flipping during polarization is more difficult, which leads to the degradation of electrical properties [16]. Therefore, the doping of KNN ceramics with appropriate BLSZ can promote the growth of ceramics grains and improve the denseness of ceramics.

As shown in Fig. 6 the elemental distribution of the ceramic sample was analyzed by EDS measurements at $x = 0.04$. All elements were detected and close to stoichiometric ratios, where the element Li has a relatively small atomic number and is a very light element, so the elemental distribution could not be detected by the electron probe [37]. The other elements were mapped on the surface by EDX analysis and the results showed that all elements were uniformly distributed in the ceramics.

Figure 7a shows the variation curves of KNN- x BLSZ ceramics dielectric constant ϵ_r and dielectric loss $\tan\delta$ with x , measured in the test frequency of 10 kHz and at room temperature. The curve of dielectric loss $\tan\delta$ with x shows fluctuations, and the dielectric constant ϵ_r shows an increase with increasing x , and then a decrease with $x > 0.04$. The KNN- x BLSZ ceramic has the best dielectric properties ($\epsilon_r = 1363$, $\tan\delta = 2.79\%$) when $x = 0.04$. The piezoelectric properties of KNN- x BLSZ ceramics with the addition of x are shown in Fig. 7b. With the increase of x , the d_{33} and k_p values show a trend of increasing and then decreasing. When $x = 0.04$, the system has the best piezoelectric properties ($d_{33} = 307\text{pC/N}$, $k_p = 46\%$). On the one hand, the superior piezoelectric properties of this ceramic system are attributed to the coexistence of R - T phase at room temperature, which can make the domain reversal during polarization easier, and on the other hand, the dense nature of the ceramic is improved by doping with BLSZ, which improves the piezoelectric properties [10]. When $x > 0.04$, the electrical properties begin to deteriorate, owing predominantly to a drop in sintering activity, which causes the tiny grains to become increasingly abundant, an elevation in domain walls and the challenge of deflection, and a fall in ceramic density.

As shown in Fig. 8a, the hysteresis loops of KNN- x BLSZ ceramics measured at 10 Hz at room temperature, it can be observed that the hysteresis loops of all component ceramics show typical ferroelectric P-E loops, and all hysteresis loops have good symmetry, from which it can be inferred that the ceramics have fewer internal defects. With the increase of x , all the P-E curves changed significantly. In order to analyze the ferroelectric properties more clearly, the remnant polarization (P_r) and coercive field (E_c) curves with x are shown in Fig. 8b. The E_c changes very little with the increase of x , and the change of E_c is related to the appearance of R phase, in addition, E_c may be influenced by grain size and domain wall mobility [7, 38]. The P_r shows a trend of increasing and then decreasing sharply, and the maximum value $P_r = 16.7 \mu\text{C/cm}^2$ is obtained at $x = 0.04$, indicating that the flip of ferroelectric domains within the ceramic will increase with the doping of BLSZ after the number of spontaneous polarization increases with the doping of BLSZ when the ceramic is in multiphase coexistence state with a lower potential barrier. When $x = 0.06$, on the one hand, the

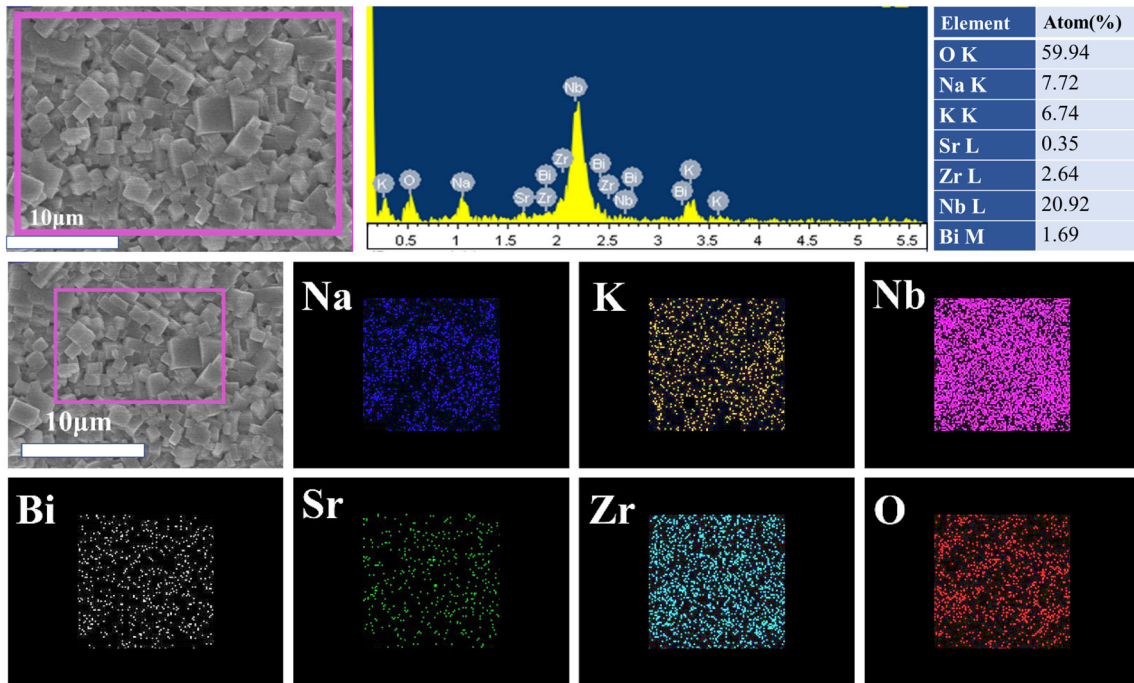


Fig. 6 Composition analysis of the cross-section and elemental mapping of the grain of KNN-xBLSZ ceramics with $x = 0.04$

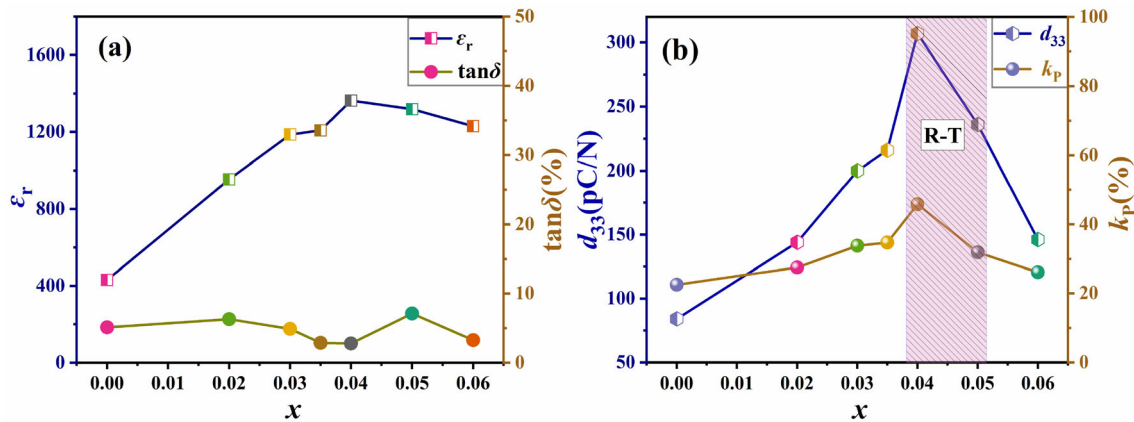


Fig. 7 **a** ϵ_r and $\tan\delta$ of the ceramics, and **b** d_{33} and k_p of the ceramics

possible explanation may be attributed to the difficulty of deflection during polarization due to grain refinement; on the other hand, it may be because of the various ionic radii and valence states of the substituted ions at A and B sites, culminating in charge imbalance and local lattice distortion, which leads to the formation of polar nano-regions (PNRs), curbing their ferroelectric properties, and potentially creating the decline of P_r [15, 19].

For ferroelectric ceramics, the relationship between the piezoelectric constant and the ferroelectric and dielectric properties can be described by the equation

($d_{33} = 2Q\epsilon_0\epsilon_r P_r$), Q and ϵ_0 are the electrostrictive coefficient and the free-space permittivity which is generally regarded as an invariant [39, 40]. ϵ_r denotes the main parameter of the polarization properties of piezoelectric materials in the presence of an electrostatic field, depending on is polarization, domain wall motion and activity of polar nanoregions (PNRs), and P_r denotes the intensity of dielectric polarization after voltage withdrawal, with the main influencing factors being the stability of the long-range ferroelectric sequence and the meritocratic

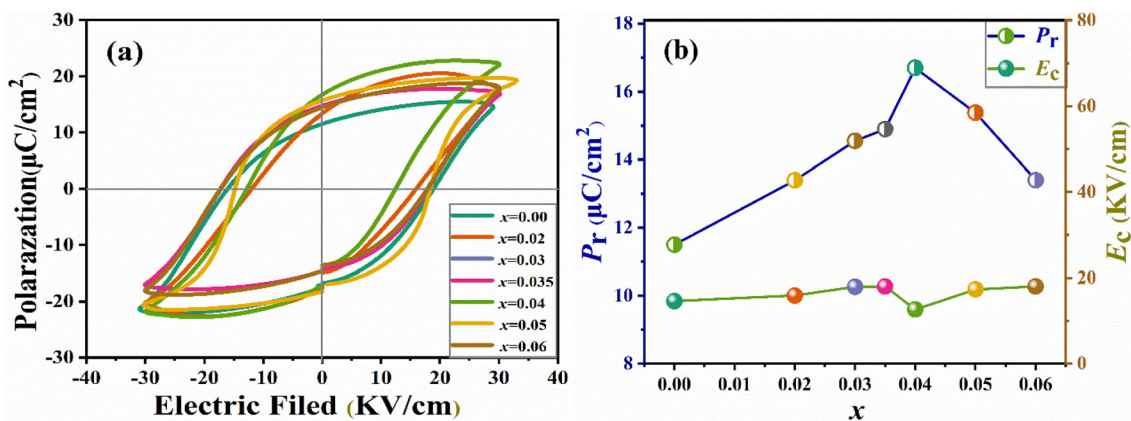


Fig. 8 **a** P–E loops of the ceramics, and **b** P_r and E_c of the ceramics

orientation of the electric domains. The piezoelectric constants (d_{33}) and $\epsilon_r P_r$ versus x for KNN- x BLSZ ceramics are plotted in Fig. 9a, and the trends of d_{33} and $\epsilon_r P_r$ can be seen to be largely fitted, the maximum value is obtained at $x = 0.04$ ($d_{33} = 307$ pC/N), which is in the state of R–T phase coexistence. Once an electric field is applied to a material for directional polarization, the flipping of ferroelectric domains within the ceramic becomes simpler, giving rise to an augmentation in the number of polarizable dipoles, which in turn leads to a rise in the polarization strength of the ceramic, which is mirrored in an increase in the dielectric and ferroelectric properties [41]. On the other hand, the enhancement of the piezoelectric properties of the ceramics are directly related to the density of the ceramics, as shown in Fig. 9b.

For practical applications of piezoelectric materials, excellent electrical properties and high T_C are indispensable to ensure their use in the temperature range.

Table 2 provides a comparison of the performance of this work with some of the reported KNN-based piezoelectric ceramics. It is observed that KNN- x BLSZ obtains superior piezoelectric properties, and it is worth mentioning that the ceramic system has an ultra-Curie temperature $T_C = 368$ °C than most of the reported ones, which is perfectly suitable for applications in higher temperature scenarios.

4 Conclusion

In this study, new high-temperature piezoelectric ceramics $(1-x)\text{K}_{0.45}\text{Na}_{0.55}\text{NbO}_3-x(\text{Bi}_{0.5}\text{Li}_{0.5})_{0.9}\text{Sr}_{0.1}\text{ZrO}_3$ were successfully prepared by the conventional solid-state method. Through modern analytical testing techniques such as XRD, SEM, and EDS, it was confirmed that the ceramics of this system in the range of $0 \leq x \leq 0.06$ ceramics formed a pure perovskite structure and all the elements were detected,

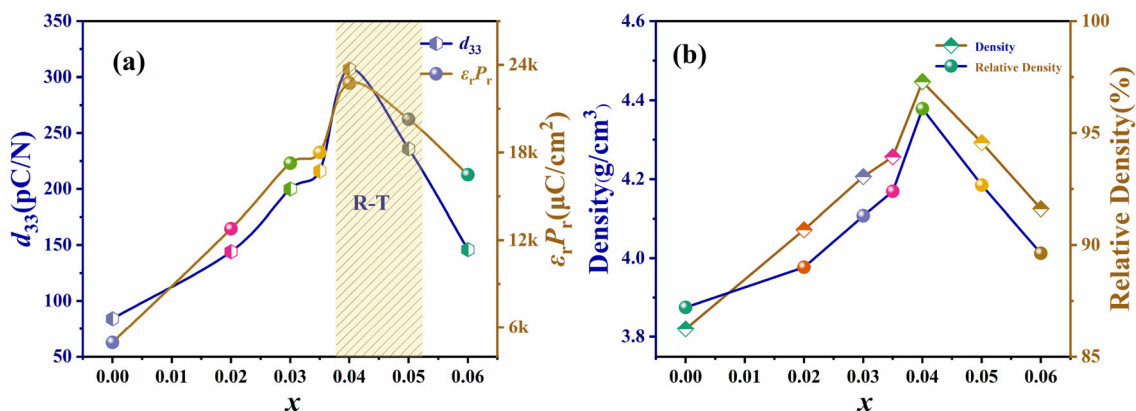


Fig. 9 **a** ϵ_r and $\tan\delta$ of the ceramics, and **b** d_{33} and k_p of the ceramics

Table 2 d_{33} and T_C of KNN-based ceramics

Materials system	d_{33} (pC/N)	T_C (°C)	References
$(1-x)\text{K}_{0.5}\text{Na}_{0.5}\text{NbO}_3-x\text{Bi}_{0.5}\text{Na}_{0.5}\text{ZrO}_3$	360	329	[42]
$(1-x)\text{K}_{0.5}\text{Na}_{0.5}\text{NbO}_3-x\text{Bi}_{0.5}\text{Na}_{0.5}\text{Zr}_{0.85}\text{Sn}_{0.15}\text{O}_3$	350	326	[43]
$(1-x)\text{K}_{0.48}\text{Na}_{0.52}\text{NbO}_3-x\text{Bi}_{0.5}\text{Ag}_{0.5}\text{ZrO}_3$	347	318	[44]
$(1-x)\text{K}_{0.5}\text{Na}_{0.5}\text{NbO}_3-x(0.15\text{Bi}_{0.5}\text{Na}_{0.5}\text{TiO}_3-0.85\text{Bi}_{0.5}\text{Na}_{0.5}\text{ZrO}_3)$	318	326	[45]
$(1-x)\text{K}_{0.45}\text{Na}_{0.55}\text{NbO}_3-x(\text{Bi}_{0.5}\text{Li}_{0.5})_{0.9}\text{Sr}_{0.1}\text{ZrO}_3$	307	368	This work

especially when the multiphase coexistence of $x = 0.04$ showed excellent electrical properties, which were $d_{33} = 307$ pC/N, $k_p = 46\%$, $\epsilon_r = 1363$, $\tan\delta = 2.79\%$, $P_r = 16.7\mu\text{C}/\text{cm}^2$, $E_c = 12.65$ kV/cm, and $T_C = 368$ °C. Therefore, we believe that the ceramics system will advance the development of KNN-based lead-free piezoelectric ceramics.

Author contributions

RZ performed the experiment and the data analyses and wrote the manuscript. QY contributed to the conception of the study. HC contributed to data curation. XZ contributed to data curation. FL contributed to data curation. YZ contributed to data curation. SW contributed significantly to analysis and manuscript preparation. ZZ contributed significantly to analysis and manuscript preparation. KH helped perform the analysis with constructive discussions. QZ helped perform the analysis with constructive discussions.

Funding

Authors gratefully acknowledge the supports of Anhui Huachen Testing Technology Research Institute Co., Ltd (Study on the modification of high-performance piezoelectric ceramics), Provincial Quality Engineering Project of Colleges and Universities of Anhui Province (Grant No. 2019jyxm1161), National grade Undergraduate Innovation and Entrepreneurship Training Project in 2022 (Grant Nos. 202211059050 and 202211059069), Natural Science Foundation of Anhui Provincial Department of Education (Grant No. 2022AH010096), and Graduate innovation and entrepreneurship

project of Hefei University in 2021 (Grant No. 21YCXL47).

Data availability

The data that support the findings of this study are available from the corresponding author upon reasonable.

Declarations

Competing interest The authors have no competing interests to declare that are relevant to the content of this article.

References

1. J. Hao, W. Li, J. Zhai, H. Chen, Progress in high-strain perovskite piezoelectric ceramics. *Mater. Sci. Eng. R Rep.* **135**, 1 (2019)
2. Y. Saito, H. Takao, T. Tani, T. Nonoyama, K. Takatori, T. Homma, T. Nagaya, M. Nakamura, Lead-free piezoceramics. *Nature* **432**, 84 (2004)
3. J. Lin, Y. Cao, K. Zhu, F. Yan, C. Shi, H. Bai, G. Ge, J. Yang, W. Yang, Y. Shi, G. Li, H. Zeng, J. Zhai, Ultrahigh energy harvesting properties in temperature-insensitive eco-friendly high-performance KNN-based textured ceramics. *J. Mater. Chem. A* **10**, 7978 (2022)
4. X. Lv, Z. Li, J. Wu, J. Xi, M. Gong, D. Xiao, J. Zhu, Enhanced piezoelectric properties in potassium-sodium niobate-based ternary ceramics. *Mater. Des.* **109**, 609 (2016)
5. B. Wu, H. Wu, J. Wu, D. Xiao, J. Zhu, S.J. Pennycook, Giant piezoelectricity and high curie temperature in nanostructured alkali niobate lead-free piezoceramics through phase coexistence. *J. Am. Chem. Soc.* **138**, 15459 (2016)
6. J. Wu, H. Tao, Y. Yuan, X. Lv, X. Wang, X. Lou, Role of antimony in the phase structure and electrical properties of

- potassium–sodium niobate lead-free ceramics. *RSC Adv.* **5**, 14575 (2015)
7. J. Xing, Z. Tan, X. Chen, L. Jiang, W. Wang, X. Deng, B. Wu, J. Wu, D. Xiao, J. Zhu, Rietveld analysis and electrical properties of BiInO₃ doped KNN-based ceramics. *Inorg. Chem.* **58**, 428 (2019)
 8. X. Yan, B. Peng, X. Lu, Q. Dong, W. Li, Structure evolution and enhanced piezoelectric properties of (K_{0.5}Na_{0.5})NbO₃–0.06LiTaO₃–SrZrO₃ lead-free ceramics. *J. Alloys Compd.* **653**, 523 (2015)
 9. K. Xu, J. Li, X. Lv, J. Wu, X. Zhang, D. Xiao, J. Zhu, Superior piezoelectric properties in potassium–sodium niobate lead-free ceramics. *Adv. Mater.* **28**, 8519 (2016)
 10. T. Zheng, J. Wu, D. Xiao, J. Zhu, Recent development in lead-free perovskite piezoelectric bulk materials. *Prog. Mater. Sci.* **98**, 552 (2018)
 11. T. Zheng, Y. Yu, H. Lei, F. Li, S. Zhang, J. Zhu, J. Wu, Compositionally graded KNN-based multilayer composite with excellent piezoelectric temperature stability. *Adv. Mater.* **34**, 2109175 (2022)
 12. X. Zhou, G. Xue, H. Luo, C.R. Bowen, D. Zhang, Phase structure and properties of sodium bismuth titanate lead-free piezoelectric ceramics. *Prog. Mater. Sci.* **122**, 100836 (2021)
 13. K. Chen, J. Ma, C. Shi, W. Wu, B. Wu, Enhanced temperature stability in high piezoelectric performance of (K, na)NbO₃-based lead-free ceramics through co-doped antimony and tantalum. *J. Alloys Compd.* **852**, 156865 (2021)
 14. X. Lv, T. Zheng, C. Zhao, J. Yin, H. Wu, J. Wu, Multiscale structure engineering for high-performance Pb-free piezoceramics. *Acc. Mater. Res.* **3**, 461 (2022)
 15. J. Wu, D. Xiao, J. Zhu, Potassium–sodium niobate lead-free piezoelectric materials: past, present, and future of phase boundaries. *Chem. Rev.* **115**, 2559 (2015)
 16. Z. Cen, W. Feng, P. Zhao, L. Chen, C. Zhu, Y. Yu, L. Li, X. Wang, Design on improving piezoelectric strain and temperature stability of KNN-based ceramics. *J. Am. Ceram. Soc.* **102**, 2675 (2018)
 17. Z. Fu, J. Yang, P. Lu, L. Zhang, H. Yao, F. Xu, Y. Li, Influence of secondary phase on polymorphic phase transition in Li-doped KNN lead-free ceramics. *Ceram. Int.* **43**, 12893 (2017)
 18. X. Wang, J. Wu, D. Xiao, J. Zhu, X. Cheng, T. Zheng, B. Zhang, X. Lou, X. Wang, Giant piezoelectricity in potassium–sodium niobate lead-free ceramics. *J. Am. Ceram. Soc.* **136**, 2905 (2014)
 19. Y. Cheng, J. Xing, C. Wu, T. Wang, L. Xie, Y. Liu, X. Xu, K. Wang, D. Xiao, J. Zhu, Investigation of high piezoelectric properties of KNNSb–Sr_xBNZ ceramics. *J. Alloys Compd.* **815**, 152252 (2020)
 20. J. Zhou, G. Xiang, J. Shen, H. Zhang, Z. Xu, H. Li, P. Ma, W. Chen, Composition-insensitive enhanced piezoelectric properties in SrZrO₃ modified (K, na)NbO₃-based lead-free ceramics. *J. Electroceram.* **44**, 95 (2019)
 21. Q. Yin, C. Wang, Y. Wang, S. Li, Q. Zhang, J. Yang, C. Tian, Structure and properties of (K_{0.5}Na_{0.5})_{0.98}Ag_{0.02}Nb_{0.96}Ta_{0.04}O₃ piezoelectric ceramics doped by CuO. *J. Mater. Sci.: Mater. Electron.* **29**, 9268 (2018)
 22. R.D. SHANNON, Revised effective ionic radii and systematic studies of interatomic distances in halides and chalcogenides. *Acta Cryst.* **A32**, 751 (1976)
 23. Y. Zhang, J.-F. Li, Review of chemical modification on potassium sodium niobate lead-free piezoelectrics. *J. Mater. Chem. C* **7**, 4284 (2019)
 24. H. Du, W. Zhou, F. Luo, D. Zhu, S. Qu, Y. Li, Z. Pei, Design and electrical properties' investigation of (K_{0.5}Na_{0.5})NbO₃–BiMeO₃ lead-free piezoelectric ceramics. *J. Appl. Phys.* **104**, 034104 (2008)
 25. K. Wang, J.-F. Li, Analysis of crystallographic evolution in (na,K)NbO₃-based lead-free piezoceramics by X-ray diffraction. *Appl. Phys. Lett.* **91**, 262902 (2007)
 26. Y. Zhang, L. Li, B. Shen, J. Zhai, Effect of orthorhombic–tetragonal phase transition on structure and piezoelectric properties of KNN-based lead-free ceramics. *Dalton Trans.* **44**, 7797 (2015)
 27. M.H. Jiang, G.Q. Zhao, Z.F. Gu, G. Cheng, X.Y. Liu, L. Li, Y.S. Du, In-depth structure characterization and properties of (1–x)(Li_{0.05}Na_{0.475}K_{0.475})(Nb_{0.95}Sb_{0.05})O₃–xBiFeO₃ lead-free piezoceramics. *J. Mater. Sci.: Mater. Electron.* **26**, 9366 (2015)
 28. W. Liu, G. Tan, P. Xiong, X. Xue, H. Hao, H. Ren, Phase transition and piezoelectric properties of (1–x)K_{0.5}Na_{0.5}NbO_{3–x}LiSbO₃ ceramics by hydrothermal powders. *J. Mater. Sci.: Mater. Electron.* **25**, 2348 (2014)
 29. H.E. Mgbemere, M. Hinterstein, G.A. Schneider, Structural phase transitions and electrical properties of (K_xNa_{1–x})NbO₃-based ceramics modified with mn. *J. Eur. Ceram. Soc.* **32**, 4341 (2012)
 30. L. Jiang, Y. Li, J. Xing, J. Wu, Q. Chen, H. Liu, D. Xiao, J. Zhu, Phase structure and enhanced piezoelectric properties in (1–x)(K_{0.48}Na_{0.52})(Nb_{0.95}Sb_{0.05})O₃–x(Bi_{0.5}Na_{0.42}Li_{0.08})_{0.9}–Sr_{0.1}ZrO₃ lead-free piezoelectric ceramics. *Ceram. Int.* **43**, 2100 (2017)
 31. B. He, Y. Du, Y. Liu, J. Wang, W. Liu, H. Xu, Phase boundary design and enhanced electrical properties in (Bi_{0.5}Li_{0.45}Ag_{0.05})(Zr_{0.98}Hf_{0.02})O₃-modified KNN-based lead-free piezoceramic. *J. Mater. Sci.: Mater. Electron.* **32**, 18240 (2021)
 32. C. Shi, J. Ma, J. Wu, X. Wang, F. Miao, Y. Huang, K. Chen, W. Wu, B. Wu, Coexistence of excellent piezoelectric

- performance and high curie temperature in KNN-based lead-free piezoelectric ceramics. *J. Alloys Compd.* **846**, 156245 (2020)
33. B. Wu, C. Zhao, Y. Huang, J. Yin, W. Wu, J. Wu, Superior electrostrictive effect in relaxor potassium sodium niobate based ferroelectrics. *ACS Appl. Mater. Interfaces* **12**, 25050 (2020)
 34. A. Munkpakdee, K. Pengpat, J. Tontrakoon, T. Tunkasiri, The study of dielectric diffuseness in the $\text{ba}(\text{Mg}_{1/3}\text{Nb}_{2/3})\text{O}_3\text{-BaTiO}_3$ ceramic system. *Smart Mater. Struct.* **15**, 1255 (2006)
 35. X. Wang, J. Wu, X. Cheng, B. Zhang, J. Zhu, D. Xiao, Compositional dependence of phase structure and electrical properties in $(\text{K}_{0.50}\text{Na}_{0.50})_{0.97}\text{Bi}_{0.01}(\text{Nb}_{1-x}\text{Zr}_x)\text{O}_3$ lead-free ceramics. *Ceram. Int.* **39**, 8021 (2013)
 36. B. Zhang, X. Wang, X. Cheng, J. Zhu, D. Xiao, J. Wu, Enhanced d_{33} value in $(1-x)[(\text{K}_{0.50}\text{Na}_{0.50})_{0.97}\text{Li}_{0.03}\text{Nb}_{0.97}\text{Sb}_{0.03}\text{O}_3] - x\text{BaZrO}_3$ lead-free ceramics with an orthorhombic-rhombohedral phase boundary. *J. Alloys Compd.* **581**, 446 (2013)
 37. H.-C. Thong, A. Payne, J.-W. Li, Y.-Y.-S. Cheng, J.L. Jones, K. Wang, The origin of chemical inhomogeneity in lead-free potassium sodium niobate ceramic: competitive chemical reaction during solid-state synthesis. *Acta Mater.* **211**, 116833 (2021)
 38. H. Wang, J. Wu, Evolution of phase structure, microstructure, and electrical properties in $(1-x)(\text{K,Na})\text{NbO}_3\text{-}x(\text{Bi,Na,Li,Ba})\text{ZrO}_3$ lead-free ceramics. *J. Alloys Compd.* **628**, 329 (2015)
 39. F. Li, D. Lin, Z. Chen, Z. Cheng, J. Wang, C. Li, Z. Xu, Q. Huang, X. Liao, L.Q. Chen, T.R. Shrout, S. Zhang, Ultrahigh piezoelectricity in ferroelectric ceramics by design. *Nat. Mater.* **17**, 349 (2018)
 40. X. Lv, N. Zhang, Y. Ma, X. Zhang, J. Wu, Coupling effects of the A-site ions on high-performance potassium sodium niobate ceramics. *J. Mater. Sci. Technol.* **130**, 198 (2022)
 41. K.-T. Lee, D.-H. Kim, S.-H. Cho, J.-S. Kim, J. Ryu, C.-W. Ahn, T.-H. Lee, G.-H. Kim, S. Nahm, Pseudocubic-based polymorphic phase boundary structures and their effect on the piezoelectric properties of $(\text{Li,Na,K})(\text{Nb,Sb})\text{O}_3\text{-SrZrO}_3$ lead-free ceramics. *J. Alloys Compd.* **784**, 1334 (2019)
 42. Z. Wang, D. Xiao, J. Wu, M. Xiao, F. Li, J. Zhu, D. Damjanovic, New lead-free $(1-x)(\text{K}_{0.5}\text{Na}_{0.5})\text{NbO}_3\text{-}x(\text{Bi}_{0.5}\text{Na}_{0.5})\text{-ZrO}_3$ ceramics with high piezoelectricity. *J. Am. Ceram. Soc.* **97**, 688 (2014)
 43. Q. Gou, J. Zhu, J. Wu, F. Li, L. Jiang, D. Xiao, Microstructure and electrical properties of $(1-x)\text{K}_{0.5}\text{Na}_{0.5}\text{NbO}_3\text{-}x\text{Bi}_{0.5}\text{Na}_{0.5}\text{Zr}_{0.85}\text{Sn}_{0.15}\text{O}_3$ lead-free ceramics. *J. Alloys Compd.* **730**, 311 (2018)
 44. X. Wang, J. Wu, X. Lv, H. Tao, X. Cheng, T. Zheng, B. Zhang, D. Xiao, J. Zhu, Phase structure, piezoelectric properties, and stability of new $\text{K}_{0.48}\text{Na}_{0.52}\text{NbO}_3\text{-Bi}_{0.5}\text{Ag}_{0.5}\text{ZrO}_3$ lead-free ceramics. *J. Mater. Sci.: Mater. Electron.* **25**, 3219 (2014)
 45. Q. Gou, D.-Q. Xiao, B. Wu, M. Xiao, S.-S. Feng, D.-D. Ma Zhao, J.-G. Wu, J.-G. Zhu, New $(1-x)\text{K}_{0.5}\text{Na}_{0.5}\text{NbO}_3\text{-}x(0.15\text{Bi}_{0.5}\text{Na}_{0.5}\text{TiO}_3\text{-}0.85\text{Bi}_{0.5}\text{Na}_{0.5}\text{ZrO}_3)$ ternary lead-free ceramics: microstructure and electrical properties. *RSC Adv.* **5**, 30660 (2015)

Publisher's note Springer Nature remains neutral with regard to jurisdictional claims in published maps and institutional affiliations.

Springer Nature or its licensor (e.g. a society or other partner) holds exclusive rights to this article under a publishing agreement with the author(s) or other rightsholder(s); author self-archiving of the accepted manuscript version of this article is solely governed by the terms of such publishing agreement and applicable law.